Kabarak Journal of Research & Innovation Volume 9 Number 1 (2020)
ISSN 2305-784X (print) ISSN 2410-8383 (online) http://eserver.kabarak.ac.ke/ojs/

Optical Modeling of Fluorine Doped Tin Oxide Films for Spectrally Selective Applications

Wycliffe M. Isoe[1*], Maxwell J. Mageto[1] and Christopher M. Maghanga[2]

[1] Department of Physics, Masinde Muliro University of Science and Technology, P.O. Box 190 Kakamega, Kenya

[2] Department of Physical & Biological Sciences, P.O. Box Private Bag Kabarak, Nakuru, Kenya

Submitted: 19th November 2019; Accepted: 10th January 2020; published online: 18th April 2020

Abstract

SnO_2: F films are widely used for solar cell applications as the front electrode as well as other applications such as electrochromic and displays. The optical design of these and other applications need knowledge of optical constants. In this study we used the dielectric constant of a combined Drude and Lorentz to model the optical behaviour of SnO_2: F using computer code created in MATLAB software. To do this, we used the fitting parameters from existing literature which were inserted into MATLAB code and *n* and *k* values were computed. Then, the *n* and *k* values were inserted into Fresnel R and T calculator and R and T spectra were computed over the 300nm -2500nm wavelength range using Fresnel's equations. We plotted n, k, T and R for different values of plasma frequency, ω_p and damping parameter, Γ. The films exhibited high visible transmittance of $> 60\%$ for all the samples and high infrared reflectance of 81.8% for the highly doped sample. The results implied the possibility of the films to be employed as spectrally selective coating materials.

KEYWORDS: Optical constants, damping parameter, thin-film, Drude-Lorentz model.

1. Introduction

Transparent conductors are materials that possess both good electrical conductivity and optical transparency in the visible portion of the electromagnetic spectrum. A wide bandgap (~>3 eV) is needed for visible transparency. A combination of transparency and conduction can be achieved in two different types of materials(Granqvist & Hultåker, 2002):- (1) Extremely thin films of metals especially Ag, Au or Cu on glass or (2) among wide-bandgap oxide semiconductors such as fluorine-doped tin oxide (FTO), antimony-doped tin oxide (ATO), tin-doped indium–oxide (ITO), niobium- doped titanium oxide (TNO) and aluminium-doped zinc oxide (AZO). Wide-band gap oxide semiconductors are in most cases referred to as transparent conducting oxides (TCOs).

TCOs have been employed technologically for more than a half-century in applications requiring both high conductivity and optical transparency. Some TCO applications include transparent electrodes for flat-panel displays (Hecht *et al*, 2011), liquid crystal displays (LCDs) (Jeong *et al*., 2006), organic light-emitting diodes (OLEDs)(Weis & Martin., 2015), as coatings for heat-reflective windows i.e. thermal management for window glass(Biswas & Prasanta, 2018), electrochromic (smart) windows (Runnerstrom, *et al*., 2014), solar cells (Boscarino, *et al*., 2014), electromagnetic shielding (Angelov, *et al*., 2015), functional glasses(Karmakar & Basudeb, 2017), electrochemical cells and gas sensors (Shim *et al*., 2011). TCOs are also applicable to transparent optoelectronics because they have the unique features of optical transparency in the visible region and controllable electrical conductivity, from almost insulating to degenerate semiconducting ($\sim 10^4$ S/cm) behaviour.

Tin oxide, among the semiconductors, demonstrates special features in chemical inertness (Mishra, *et al.*, 2009), stability to heat treatment and mechanical hardness. Further, tin oxide films are highly transparent in the visible range (Chitra, *et al.*, 1991). It also has a direct bandgap of approximately 3.6eV(Shanting, 2017) which makes it possible to have a wide range of applications in electronic devices. In order to improve its optical and electrical properties, tin oxide films need to be doped with the right dopants such as fluorine, cadmium, molybdenum and

[*] *Corresponding author e-mail: *e-mail: isoewycliffe@gmail.com*

antimony (Wang ,*et al.*, 2019). Among these dopants, fluorine is found to be the best dopant for tin oxide since the radii of O^{2-} and F^{-} are similar hence there will be no mismatch of lattices during doping (Wang ,*et al.*, 2019).
Thin films of transparent oxide semiconductors, such as F-doped tin oxide, are widely investigated due to their high optical transmission, electrical conduction, and infrared reflection. These properties make these films to find wide applications in optoelectronic devices, hybrid microelectronics, photothermal conversion and direct energy conversion devices particularly in conductor-insulator- semiconductor solar cells. Fluorine-doped tin oxide has a work function of about 4.9eV, electron concentration in the order of $10^{20}cm^{-3}$, an approximate minimum resistivity of about $200\mu\Omega cm$ and a visible absorption coefficient of about 0.04(Roy & Gordon, 2000).

Thin-film surface coatings are most widely employed for the efficient conversion of solar radiation into other useful forms, such as thermal energy for heating and cooling applications; and electrical energy by direct conversion using photovoltaic cells. The other current applications of such optical coatings include: transparent heat mirrors (Dobrikov, *et al.*, 2009), antireflection coatings(Ronard & Willey, 2016), architectural coatings(Thelen, 1981), photo-thermal converters(Thelen, 1981), and photocatalysis(Nakata & Fujishima, 2012).

Invar Hamberg (1984) in his thesis(Ivar, 1984), reported that for the material to be used as spectrally selective coating material, it must meet three conditions: (1) should have a significantly wide band gap in order for the material to guarantee the key absorption edge to be below a solar wavelength length of approximately 300nm; (2) a prospect to dope the material to attain a high free carrier concentration leading to a high infrared reflectivity; (3) a limited absorption between the key absorption edge and the plasma wavelength, to guarantee a high luminous transmittance. Also, Maghanga in his thesis(Maghanga, 2009) reported separately that for a material to be used as a spectrally selective reflector (SSR), it must exhibit very high visible transmittance and high infrared reflectance. Furthermore, he suggested that the region of the plasma absorption peak must be positioned in the part of the solar spectrum with photon energies lower than the bandgap of the given solar cell. Spectrally selective films are those films that allow peculiarly selected portions of the light spectrum to pass through a medium while blocking some i.e. their transmission and/or reflection properties are regulated for selected and controlled packages of thermal radiation fluxes(Wanga & Shi, 2017). The conditions aforementioned necessitated the need to investigate a thin film that would meet all the conditions. Thus, the main aim of the study was to optically model fluorine doped tin oxide films for spectrally selective applications

There are apparently many methods that have been employed to study the optical behaviour of SnO_2: F films as it is the case in numerous publications. The appropriate investigation of the optical properties of the films requires the finding of optical constants such as the extinction coefficient, k and refractive index, n over the desired wavelength range. In the present work, we employed the dielectric constant of a combined Drude and Lorentz to investigate the optical properties of SnO_2: F films.

1.1 Theoretical Background

The absorption and refraction of a medium can be described by a single quantity called complex refractive index(Mark, 2001). This is usually given the symbol $\tilde{n}$ or N and is defined as shown in equation (1).

$$N = n + ik \quad [1]$$

The real part of N namely n is the same as the normal refractive index defined in equation (2). The imaginary part of N, namely k, is called the extinction coefficient which is related to the absorption coefficient as shown in equation (3).

$$n = \frac{c}{v} \quad [2]$$

$$\alpha = \frac{2\omega k}{c} = \frac{4\pi k}{\lambda} \quad [3]$$

The complex refractive index of any medium can be related to the complex dielectric constant by using equation (4). This shows that if *n* is complex, then ε must also be complex.

$$N^2 = \tilde{\varepsilon}_r = \varepsilon_1 + i\varepsilon_2 \quad [4]$$

By comparing equations (1) and (4), explicit relationships between the real and imaginary parts of N and $\tilde{\varepsilon}$ can be computed and the resulting equations are as shown in equations (5) and (6).

$$\varepsilon_1 = n^2 - k^2 \quad [5]$$

$$\varepsilon_2 = 2nk \quad [6]$$

Here *n*, *k*, e_1 and ε_2 are referred to as the optical 'constants' of the medium. They are referred to as constants due to historical reasons otherwise they are functions of wavelength. ε_1 is related to the polarizability and ε_2 to the true optical absorption. These values depend on the photon energy, $E = \hbar\omega$. Further, these optical constants, for any medium, can be calculated from a Drude-Lorentz model given in equation (7) (Kadi, *et al.*, 2012). The individual Drude and Lorentz models are as given in equations (8) and (9) respectively.

$$\varepsilon = \varepsilon_\infty - \frac{\omega_D^2}{\omega^2 + i\Gamma_D\omega} + \frac{\omega_L^2}{\left(\omega_0^2 - \omega^2\right) - i\omega\Gamma_L} \quad [7]$$

$$\varepsilon_r'(\omega) = 1 - \omega_p^2 \cdot \frac{1}{\omega^2 + \Gamma^2}, \qquad \varepsilon_r''(\omega) = \omega_p^2 \frac{\Gamma/\omega}{\omega^2 + \Gamma^2} \quad [8]$$

$$\tilde{\varepsilon} = 1 + \frac{Ne^2}{\varepsilon_0 m} \frac{1}{\left(\omega_0^2 - \omega^2\right) - i\omega\Gamma} \quad [9]$$

The Fresnel equations that are usually used to work out the transmittance and reflectance of the films are as shown in equations 10-19(Ribbing, 2002).

$$t_p = \frac{2N_1\cos\theta_1}{N_1\cos\theta_2 + N_2\cos\theta_1} \quad [10]$$

$$t_s = \frac{2N_1\cos\theta_1}{N_1\cos\theta_1 + N_2\cos\theta_2} \quad [11]$$

$$r_p = \frac{N_2\cos\theta_1 - N_1\cos\theta_2}{N_2\cos\theta_1 + N_1\cos\theta_2} \quad [12]$$

$$r_s = \frac{N_1\cos\theta_1 - N_2\cos\theta_2}{N_1\cos\theta_1 + N_2\cos\theta_2} \quad [13]$$

And at normal incidence the equations become:

$$r_1 = \frac{N_2 - N_1}{N_2 + N_1}, \; r_2 = \frac{N_3 - N_2}{N_3 + N_2} \quad [14]$$

$$t_1 = \frac{2}{N_1 + N_2}, \; t_2 = \frac{2N_2}{N_2 + N_3} \qquad [15]$$

Hence, r and t can be found according to:

$$r = \frac{r_1 + r_2 e^{-2i\partial}}{1 + r_1 r_2 e^{-2i\partial}} \qquad [16]$$

$$t = \frac{t_1 t_2 e^{-i\partial}}{1 + r_1 r_2 e^{-2i\partial}} \qquad [17]$$

where the phase shift, ∂, is given by

$$\partial = -\frac{2\pi}{\lambda} N_2 d\cos\theta_2, \text{ which for normal incidence becomes; } \partial = -\frac{2\pi N_2}{\lambda} d \qquad [18]$$

and r_1 and t_1 are the Fresnel coefficients for the boundary between air and film and $r_2$and t_2 are the corresponding coefficients for the boundary between film and substrate.

With the Fresnel equations above, the intensity reflectance, R, and the intensity transmittance, T, can be calculated according to:

$$R = rr^* \quad \text{and} \quad T = \mathrm{Re}\left(\frac{N_3}{N_1}\right) tt^* \qquad [19]$$

where r^* is the conjugate of the amplitude reflectance and t^* is the conjugate of the amplitude transmittance.

2. The Simulation Method.

The Drude–Lorentz modelling of optical spectra of SnO_2: F films were simulated using equation (7) which was implemented in a computer code that was created in MATLAB software. To do this, we used the fitting parameters from literature shown in table (1) which were inserted into the MATLAB code from which *n* and *k* values, as well as the real part (ε_1) and imaginary part (ε_2) were computed. Then, each pair of *n* and *k* values were inserted into Fresnel equation R & T calculator together with Fresnel's equations (equations 10-19), which is MATLAB code created in MATLAB software, to compute R- and T- spectra of SnO_2: F films at different film thicknesses, d and for the various doping concentrations, n_e, over 300 – 2500nm wavelength range. Different values of plasma frequencies, $\omega_p\left(s^{-1}\right)$, were used as shown in table 2. All the simulation was done by using the MATLAB codes created in MATLAB software.

The figures shown below represent the modelled optical data for the different samples i.e. S_A, S_B, S_C, S_D, S_E, S_F and S_G. S_A is the undoped sample whereas S_G is the heavily doped sample. The dopant concentration was increased gradually by varying the value of $\omega_p\left(s^{-1}\right)$ as depicted in table 2.

Table 1. **Drude and Lorentz parameters for undoped and F-doped tin oxide**

	ε_∞	$\omega_p\left(\times`10^{14}s^{-1}\right)$	$\Gamma_D(eV)$	$\omega_p\left(s^{-1}\right)$	$\Gamma_L(eV)$	$\omega\left(s^{-1}\right)$
SnO_2	4.0	-	-	$1.56\times`10^{14}$	0.5064	$8.19\times`10^{14}$

SnO_2: F	3.19	1.43	0.167	$24.67\times`10^{15}$	0.1275	$1.27\times`10^{15}$

Table 2: Values of plasma frequencies, $\omega_p\left(s^{-1}\right)$ used to calculate the optical constants in a combined Drude and Lorentz model.

Sample	S_A	S_B	S_C	S_D	S_E	S_F	S_G
$\omega_p\left(\times`10^{14}s^{-1}\right)$	0	1.43	2.02	2.85	3.49	4.03	5.71

3.Results and Discussion

3.1 Optical Studies

In order to compare the reflectance and transmittance of SnO_2 thin films with various F-doping levels, the optical R- and T-spectra in the UV-VIS-NIR region of the samples were computed and the results are shown in Figures 1 (a), (b), (c)and (d). The various film thicknesses shown in figures 1 (a), (b) and (c)are meant to magnify the optical properties of the graphs in the near IR for easy comparison.

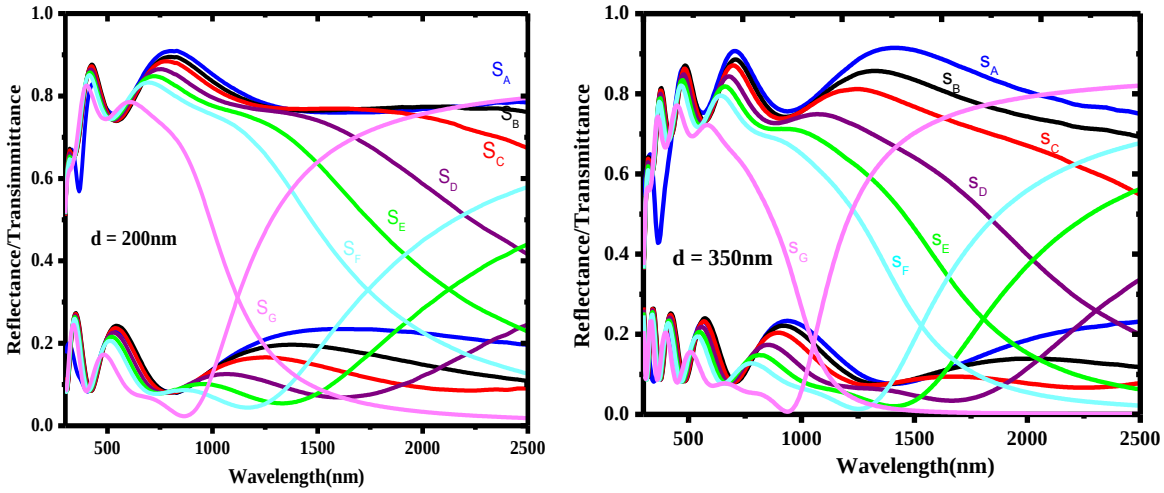

(a) (b)

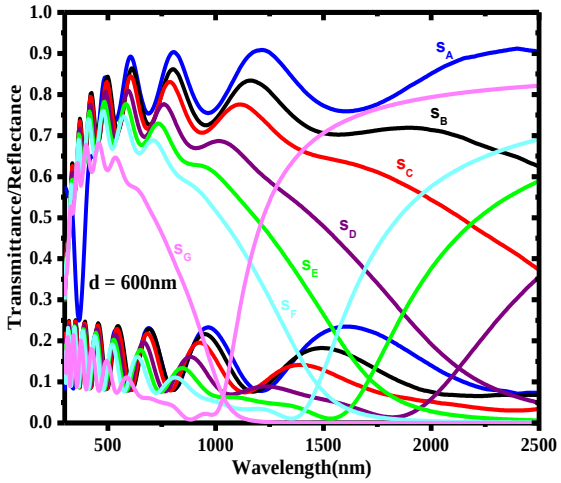

(c)

Figure 1 Spectral reflectance and transmittance for various F-doping concentrations at various film thickness (a) d = 200nm, (b) d = 350nm, (c) d = 600nm.

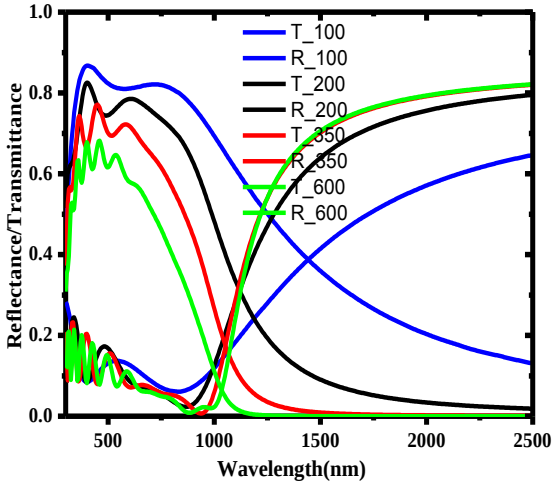

Figure 1(d) Spectral reflectance and transmittance of the highly doped sample (S_G) showing various film thicknesses. The films thicknesses were 100nm, 200nm ,350nm and 600nm.

It is clearly noted from the figures 1 (a), (b) and (c) that the films exhibit high transmittance in the visible region but in near IR region the transmittance starts to decrease with increase in F-doping concentration. The decrease in transmittance is due to reflection by the free electron in the highly F- doped SnO_2. This further illustrates that although doping improves the free carrier concentration thus the conductivity, it jeopardizes the transmittance of the films. Thus, there is a demand that a compromise between the optical properties and electrical properties should be attained for TCOs. On the other hand, reflectance increases in the near-infrared region with increasing F doping concentration to a maximum of 81.8% for the highly doped sample. The reduction of transmittance and the rise of reflectance at near-infrared indicate that the samples start to conduct. These observations are perfectly in agreement with other already reported work (Shadia, *et al.*, 2008). The transmittance and reflectance behaviour of the films at various F-doping levels illustrates that doping improves the optical properties as well as conductivity of the films to a significant degree.

The shifts in the transmittance and reflectance fringes of the doped samples propose that doping leads to a slight change in the thickness and in the refractive index of the films. This can be verified by using the number of

interference fringes as given in equation 20(Swinepoxes, 1983) and by Swanepoel formula given in equation 21(Theiss & Teiss, 2001) respectively.

$$d = \frac{\lambda_1 \lambda_2}{2(\lambda_1 n_1 - \lambda_2 n_1)} \quad [20]$$

where n_1 and n_2 are refractive indices at two adjacent maxima (or minima) at λ_1 and λ_2 respectively.

$$n = \sqrt{N + \sqrt{N^2 - S^2}} \quad [21]$$

where

$$N = 2S\frac{T_M - T_m}{T_M T_m} + \frac{S^2 + 1}{2} \quad [22]$$

where S is the refractive index of the substrate, T_M and T_m represent the maximum and minimum transmittance envelopes at the fringes.

It is also noted from the figures that there is the cross over between R and T curves which shifts towards the visible range with increasing fluorine doping. These cross over show the position of the plasma wavelength. The plasma frequency ω_p, which according to classical Drude is as given in equation 23, is used to characterize the reflection by the free carriers. Using equation 23 we computed the carrier concentration, n_e of the samples and their corresponding values were recorded as shown in tables 3 and 4.

$$\omega_p = \left(\frac{n_e e^2}{\varepsilon_0 \varepsilon_\infty m^*}\right)^{\frac{1}{2}} \quad [23]$$

where ε_0 is the permittivity of free space, ε_∞ the high-frequency dielectric constant and m^* the effective conduction –band mass. In this paper, we assumed the value of $m^* = 0.25m_e$ (Kulkarnia, Kirk, Schultz, Khan, & Lima, 1999) where m_e is the free electron mass.

The Spectral reflectance and transmittance at different film thicknesses were also investigated and the results are as shown in figure 1(d). The film thicknesses were increased from 100nm up to 600nm. It was clearly noted that increasing film thickness leads to an increase in reflectance and a decrease in transmittance. This observation is evidence that the film thickness significantly affects the transmittance and reflectance characteristics.

The optical constants i.e. spectral refractive index $n(\lambda)$, extinction coefficient $k(\lambda)$, real (ε_1) and imaginary (ε_2) parts of the dielectric constant for SnO_2 and SnO_2 : F films are reported as shown in figures 2, 3, and 4 respectively. From figure 2 it was clear that the undoped film shows a dielectric behaviour with n = 2 over the 300nm -2500nm wavelength range. This value is well comparable with 1.98 already reported(Shamala., 2004). This refractive index value makes the transparent semiconducting tin oxide suited to be employed as an inherent antireflection coating on silicon(Maudes & Rodrigues, 1980).

From figures 3 and 2 it is clearly noted that $k(\lambda)$ increases with an increase in wavelength whereas $n(\lambda)$ shows a decrease towards higher wavelengths. These effects are more pronounced with increasing F-doping concentration. This behaviour was as expected for the case of metallic materials (Mageto, *et al.*, 2015) and it may be associated to both shift of the plasma edge as well as the Burstein- Moss shift of the band edge(Mergel & Qiao, 2002).

Figures 4 show that ε_1 decreases with increasing fluorine doping concentrations while ε_2 shows an increase. It is also clearly noticed that the real dielectric constant, ε_1 is substantially negative in the wavelength range of high reflectance. This can be understood to mean that high negative values of ε_1 match with a phase relationship between the light and polarization. This relation aligns the polarization in the opposite direction to the incoming electromagnetic wave and hence high reflectance.

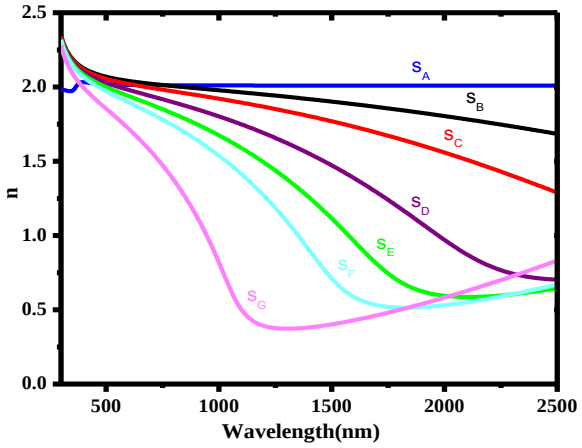

Figure 2. Spectral refractive index, $n(\lambda)$ for the SnO_2 and SnO_2: F for various levels of F-doping concentration.

Comparing figures 2 and 4(a), it is clearly noted that the real refractive index, *n*, is small over the region where ε_1 is negative. This makes the material to be optically metal-like (Mageto, *et al.*, 2012). This further informs us that when ε_1 is negative, the optical constants are $n \approx 0$ and $k = \sqrt{-\varepsilon}$ corresponding to an exponentially damped field without energy loss, $\varepsilon_2 = 0$ (Wooten, 1972).

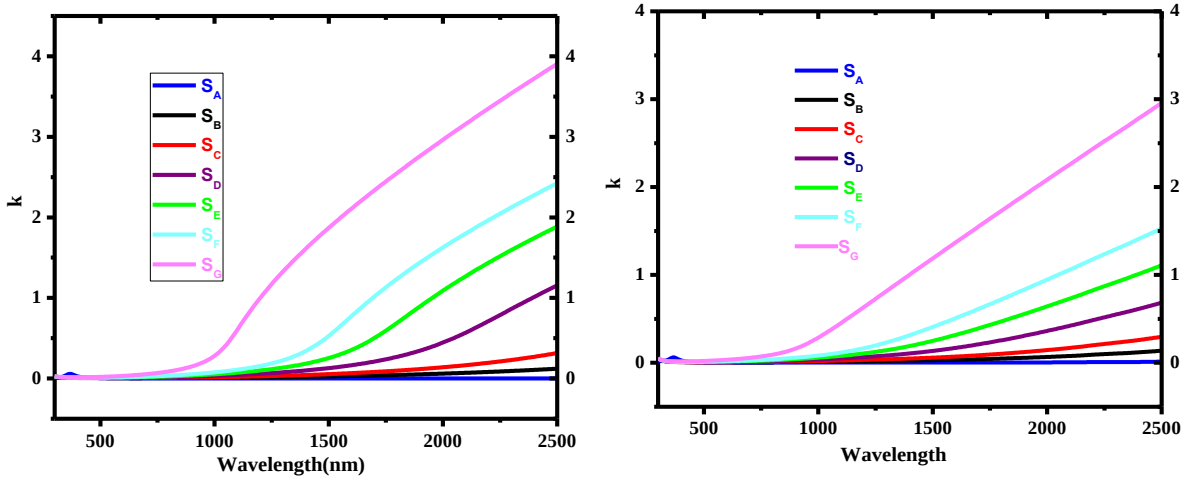

(a) (b)

Figure 3. Spectral extinction coefficient, $k(\lambda)$ for the SnO_2 and SnO_2: F showing values of k calculated from (a) Drude-Lorentz model and (b) Hong's formula at d = 350nm.

Figures 3 show a comparison of the spectral extinction coefficient, $k(\lambda)$ between the various values of k computed from the Drude - Lorentz model and that from Hong's formula. Hong's formula that was used to compute the *k* values is as shown in equation 24(Hong, 1989). The slight difference observed may be due approximation and assumption nature of the formulae.

$$\frac{1-R}{T} = \exp\left(\frac{4\pi kd}{\lambda}\right) \qquad [24]$$

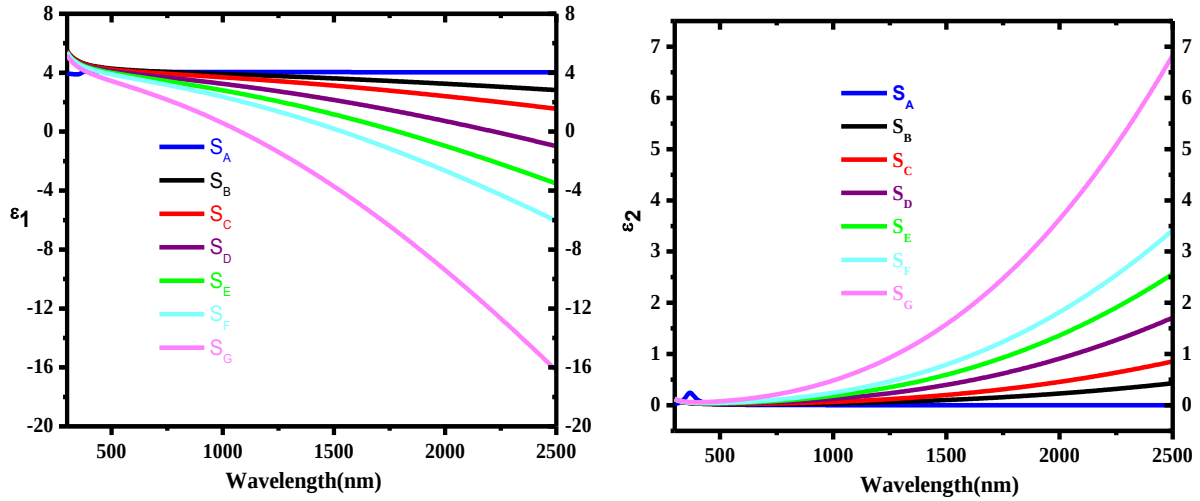

(a) (b)

Figure 4. The real part of dielectric constant, ε_1 and the complex dielectric constant, ε_2 versus wavelength.

Table 3: Carrier concentration, n_e values at different plasma frequencies for the samples at d = 350nm

Sample	Plasma frequency, ω_P $(\times 10^{15} s^{-1})$	Plasma wavelength, λ_P (nm)	Carrier concentration, $(\times 10^{20} cm^{-3})$
S_D	0.81916	2301.08	1.6817
S_E	1.0422	1808.60	2.7223
S_F	1.2354	1525.81	3.8249
S_G	1.7870	1054.84	8.0029

Table 4: Carrier concentration, n_e values at different film thickness.

Thickness d(nm)	Sample	Plasma frequency, ω_P $(\times 10^{15} s^{-1})$	Plasma wavelength, λ_P (nm)	Carrier concentration, $(\times 10^{20} cm^{-3})$
100	S_D	1.3043	1445.16	4.2637
200	S_E	1.6905	1115.05	7.1619
350	S_F	1.7870	1054.84	8.0029
600	S_G	1.8166	1037.63	8.2705

Using values in tables 3 and 4 we drew the graphs of carrier concentration, n_e as a function of plasma frequency, ω_P . The graphs are as shown in figures 5. It is clearly noted from the figures that the carrier concentration of all the

samples increases linearly with increasing plasma frequency, ω_p. This further makes it clear that it is the carrier concentration that shifts the plasma edges towards the visible range as was shown in figures 1.

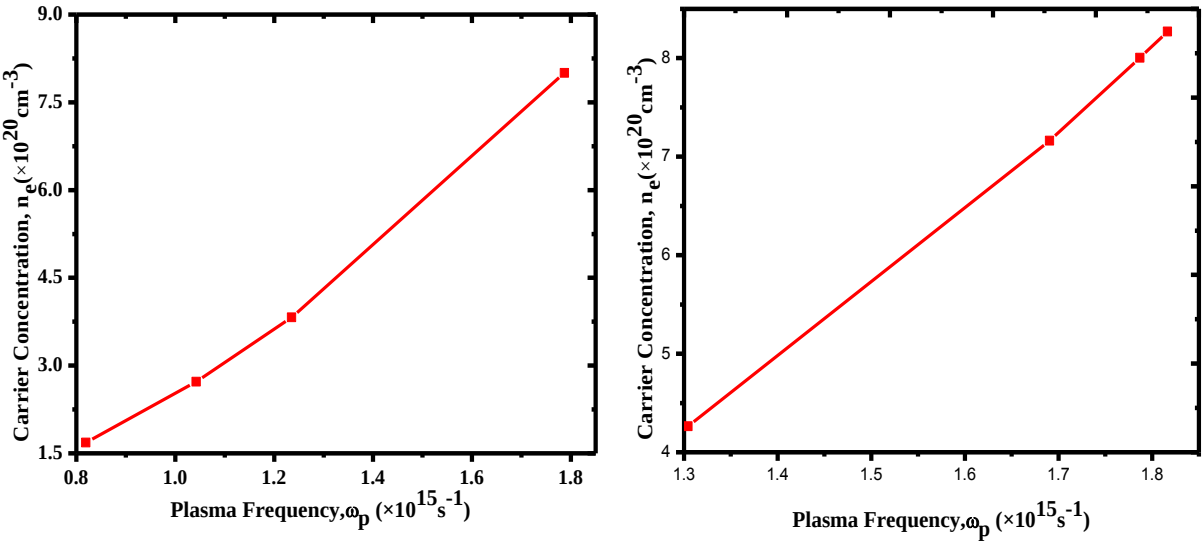

(a) (b)

Figure 5. Carrier concentration against wavelength showing (a) various plasma frequencies of the samples and (b) various film thicknesses of the samples.

The optical bandgap E_g was evaluated from the standard expression(Granqvist C. , 1995).

$$\alpha h v \propto (h v - E_g)^m \quad [25]$$

where h is Planck's constant, v is the frequency and hence hv is the photon energy in electron-volts (eV) and $\alpha = \frac{2\pi k}{\lambda}$ is the absorption coefficient. The constant *m* depends on the optical transition mode having the values as listed in Table 4.

The Plots of $(\alpha h\nu)^{\frac{1}{2}}$ versus photon energy, $h\nu$, in the high absorption region, and extrapolation of the curve to $h\nu$ axis gives the indirect band gap. Similarly, $(\alpha h\nu)^2$ versus $h\nu$ and extrapolating to the hv axis gives a direct bandgap. Tin oxide is a direct bandgap material (Shanthi, Dutta, Banerjee, & Chopra, 1980).

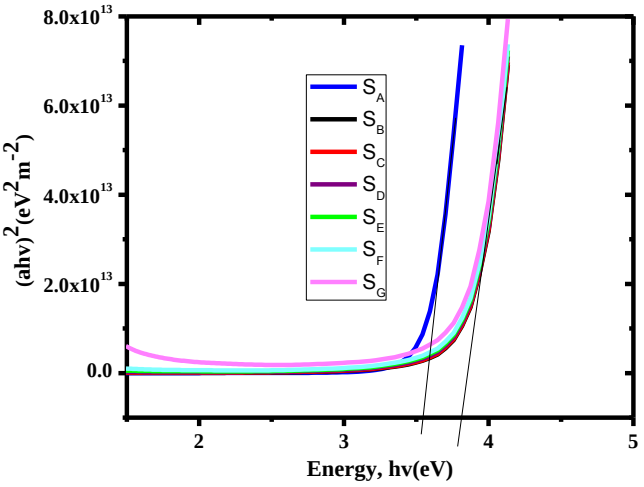

Figure 6. $(\alpha hv)^2$ Verses hv plots for determining the optical direct band gap of SnO_2 and SnO_2: F.

Figure 6 shows plots of $(\alpha hv)^2$ versus photon energy, hv in high absorption region. Extrapolation of the curves to hv = 0 gave the direct band of SnO_2 and SnO_2: F films in the range 3.55eV – 3.81eV for the undoped and heavily doped films. It was found out that the direct band gap for SnO_2 to be 3.55 eV which compares well with 3.6eV as already reported(Zhang, 2017).

Further, it is noted that there is a widening of bandgap with increase of fluorine doping concentration. This widening of the bandgap can be understood on the basis of Burstein–Moss shift, which occurs due to filling up of low-lying energy levels by the conduction electrons(Hamberg & Granqvist). According to this well-known Burstein-Moss (BM) shift, above the Mott critical density the partial filling of the conduction band causes a blocking of the lowest states and thus a widening of the optically observed bandgap. Further, above the Mott critical density, the valence and conduction bands are shifted in energy as a result of electron-electron and electron-impurity scattering(Ivar, 1984). In SnO_2 these incline to partially compensate the BM shift.

Now, assuming the function of electron-electron and electron-impurity scattering, the energy gap for direct transitions in the doped material is given in terms of the unperturbed bands as shown in equation 26(Ivar, 1984).

$$E_g^o = E_c^o(k_F) - E_v^o(k_F) \quad [26]$$

Alternatively, equation (26) may be expressed as shown in equation (27)

$$E_g^o = E_{g0} + \Delta E_g^{BM} \quad [27]$$

where the BM shift is given by equation (28)

$$\Delta E_g^{BM} = \frac{\hbar^2}{2m_{vc}^*}\left(3\pi^2 n_e\right)^{2/3} \quad [28]$$

with the reduced effective mass according to equation (29)

$$\frac{1}{m_{vc}^*} = \frac{1}{m_v^*} + \frac{1}{m_c^*} \quad [29]$$

Equation (29) predicts an energy gap shift proportional to $n_e^{2/3}$. Using equation (28) the values of BM of the samples S_D, S_E, S_F and S_G. were computed. The computed values were 2.7736×10^{18}eV , 3.8238×10^{18}eV , 4.7968×10^{18}eV and 7.8470×10^{18}eV respectively. From the values, it is clear that the optical bandgap should increase.

Table 4: Values of the exponent m for Equation 25 for different band gap transition modes.

	Transition mode
½	Direct allowed
3/2	Direct forbidden
2	Indirect allowed
3	Indirect forbidden

Figure 7 shows absorption spectra over the wavelength range 300 – 2500nm for the samples in figure 1(c). The absorption for each sample was calculated from the relation in equation (30). It was noted that almost all the samples have an absorption peak which shifts towards the visible wavelength range with increase in fluorine doping concentration. The shift of the position of the absorption edge can be associated with the varying bandgap.

$$T + R + A = 1 \qquad [30]$$

where T is the transmittance, R is the reflectance and A is the absorption.

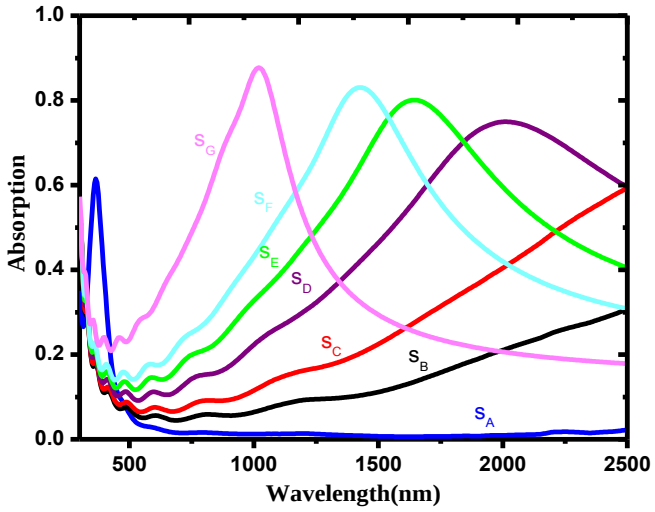

Figure 7. Spectral absorptance A = 1-(R+T) for the samples in figure 1.0 (c).

3.2Electrical Studies.

The relationship between electrical conductivity and the optical constants is as given in equation (31)(Wooten, 1972).

$$\frac{\sigma_1}{c} = \frac{nk}{\lambda_0}, \qquad [31]$$

where $\lambda_0 = \frac{2\pi c}{\omega_0} = 12,850\text{nm}$.

Using the relation in equation (31) the electrical conductivity, σ_1 was computed for all the samples and the results are presented as shown in figure 8. It is observed from the figure 8 that the electrical conductivity increases exponentially with increasing dopant concentration. This observation illustrates that doping improves the conductivity properties of the material to a significant degree.

From figures 4(b) and 8 it is clearly observed that there is a close relationship between the optical conductivity, σ_1 and the imaginary part of the dielectric constant, ε_2.

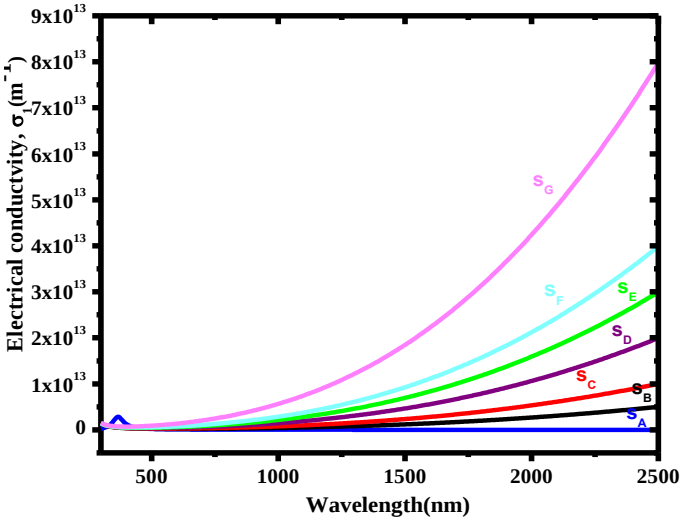

Figure 8. Electrical conductivity spectra

4. Conclusion

In this work, fluorine-doped tin oxide films were modeled successfully using a dielectric constant of a combined the Drude and Lorentz model. From the analysis, it was shown that the films had high visible transmittance of $> 60\%$ for all the samples and high infrared reflectance of 81.8% for the highly doped sample. The results imply the possibility of the films to be employed as spectrally selective coating materials. From the analysis, it can be concluded that an increase in the doping concentration improves the optical and electrical properties of tin oxide to a greater extent. From the study it can also be concluded that the film thickness also affects the transmittance and reflectance properties of the films. An increase in film thickness leads to an increase in reflectance and a decrease in transmittance. From the study of the optical constants it can also be concluded that, in practice, it is only ε_1 that be negative.

Acknowledgement

The authors most sincerely appreciate Masinde Muliro University of Science and Technology for the conducive research environment they accorded us in the process of carrying out this study.

References

Angelov, K., Komitov, H., & Mustafov, A. (2015). Transparent conductive oxides and their shielding efficiency against electromagnetic interferences. 111-115.

Biswas, & Prasanta, K. (2018). Study of solar radiation at various incident angles on soft chemistry based transparent conducting oxide (TCO) coated window glass. *Journal of Fundamentals of Renewable Energy and Applications*, 57-65.

Biswas, P. K. (2018). Study of solar radiation at various incident angles on soft chemistry based transparent conducting oxide (TCO) coated window glass. *Journal of Fundamentals of Renewable Energy and Applications*, 57-65.

Boscarino, S., Crupi, I., Mirabella, S., Simone, F., & Terassi, A. (2014). TCO/Ag/TCO transparent electrodes for solar cells application. *Applied Science A*, 1287–1291.

Chitra, A., Takwale, M., Bhide, V., Shailaja, M., & Kulkarni, S. (1991). Effect of Sn incorporation on the growth mechanism of sprayed SnO2 films. *American Instute of Physics*, 73-82.

Chitra, T., Bhide, S., & Kulkarni. (1991). Effect of Sn incorporation on the growth mechanism of sprayed SnO2 films. *Amerrican Instute of Physics*, 73-82.

Chitra, Takwale, Bhide, Shailaja, & Kulkarni. (1991). Effect of Sn incorporation on the growth mechanism of sprayed SnO2 films. *Amerrican Instute of Physics*, 73-82.

Dobrikov, G., Rassovska, M., Andreev, M., Boyadzhiev, S., & Gesheva, K. (2009). Development of transparent heat mirrors based on metal oxide thin film structures. *Thin Solid Films*, 1091-1094.

Granqvist, C. (1995). *Handbook of Inorganic Electrochromic Materials.* the Netherlands: Elsevier, Amsterdam.

Granqvist, C., & Hultåker, A. (2002). Transparent and Conducting ITO Films: New Development and Applications. 1-5.

Hamberg, I., & Granqvist, C. (n.d.). *Appl. Phys*.

Hecht, Hu, D., & Irvin, G. (2011). Emerging Transparent Electrodes Based on Thin Films of Carbon Nanotubes, Graphene and Metallic Nanostructures. *Advanced materials*, 1482-1513.

Hong, W. (1989). Extraction of extinction coefficient of weak absorbing thin films from special absorption. *Journal of Applied Physics D: Applied Physics, 22*, 1384-1385.

Ivar, H. (1984). *Indium-Tin-Oxide Thin Films:Basic Optical Properties and applications to Energy Efficient Windows.* Goteborg, Sweden: Chalmers University of Technology.

Jeong, B.-Y. &., Moon, M.-C. &., Lee, T.-H. &., Myoung, W. &., Hwang, J.-M. &., Jeoung-Yeon, . . . Dae-Shik. (2006). Transparent conductive Al-doped ZnO films for liquid crystal displays. *Journal of Applied Physics*(99), 124505-124505.

JI, S., & NAB, R. (2008). Effect of Processing on the Electrical Properties of Spray-Deposited SnO2:F Thin Films. *Journal of Applied Science*, 672-677.

Kadi, M., Smaali, A., & Outermzabet, R. (2012). Analysis of Optical and related properties of tin oxide thim films determined by Drude-Lorentz model. *Surf.Coat.Technol., 211*(45), 1-7.

Karmakar, & Basudeb. (2017). *Functional Glasses and Glass-Ceramics.* United Kingdom: Butterworth-Heinemann.

Kulkarnia, A., Kirk, H., Schultz, T., Khan, M., & Lima. (1999). Dependence of the Sheet resistance of Indium-tin-oxide thin films on grain size and grain orientation determined from x-ray diffraction. *Thin solid films*, 273-277.

Mageto, Maghanga, C., Mwaburi, M., & Jafri, H. (2015). Transparent and conducting TiO2:Nb thin films prepared by spray pyrolysis technique. *American Research Journal of Physics*, 63.

Maghanga, C. (2009). Preparation and Characterisation of a Spectrally Selective Reflector Surface Based on TiO2: Nb Thin Films. *Unpublished Ph.D Thesis*. Eldoret: Moi University.

Mark, F. (2001). *Optical Properties of Solids.* New York: Oxford University Press.

Maudes, J., & Rodrigues, T. (1980). Sprayed SnO2 films: Growth Mechanism and film Structure Characterization. *Thin film solids*, 183-189.

Mergel, D., & Qiao, Z. (2002). Dielectric modelling of the optical spectra of thin In2O3:Sn films. *Journal of Physcics D: Applied Physics*, 794-801.

Mishra, R., Sheo, K., & Prakash, G. (2009). Optical and gas sensing characteristics of tin oxide nano-crystalline film. *Journal of Ovonic Research*, 77-85.

Nakata, K., & Fujishima, A. (2012). TiO2 photocatalysis:Design and applications. *Journal of Photochemistry and photobiology C*, 169-189.

Ribbing, C. G. (2002). *Introduction to Material Optics, a Compendium.* Sweden: Uppsala University.

Ronard, R., & Willey. (2016). Thin-film Coatings: Understanding key design principles of antireflection coatings. *Laser Focus World*.

Roy, G., & Gordon. (2000). Criteria for choosing Transparent conductors. *MRS Bulletin*, 52-57.

Runnerstrom, L., Lorde, A., Lounisac, D., & Milliron, J. (2014). Nanostructured electrochromic smart windows: traditional materials and NIR-selective plasmonic nanocrystals. *Royal society of chemistry*, 10555-10572.

Shadia, J, & Riyad, N. (2008). Effect of Processing on the Electrical Properties of Spray-Deposited SnO2:F Thin Films. *Journal of Applied Science*, 672-677.

Shamala. (2004). Studies on Tin oxide Films Prepared by Electron Beam Evaporation and Spray Pyrolysis Methods. *Indian Academy of Sciences, Bull. Material Sci.*, 295-301.

Shanthi, E., Dutta, V., Banerjee, A., & Chopra, K. (1980). Electrical and Optical Properties of undoped and antimony-doped tin oxide films. *Journal of Applied Science*, 6243-6253.

Shanting, Z. (2017). Study of fluorine-doped tin oxide (FTO) thin films for photovoltaics applications. *Materials Universite Grenoble*, 40.

Shim, Y., Moon, G., Kim, H., Jang, W., & Kang, C. (2011). Transparent conducting oxide electrodes for novel metal oxide gas sensors. *Elsevier, Sensors and Actuators B*, 357-363.

Swinepoxes, R. (1983). Determination of Thickness and Optical Constants of Armorphous Silicon. *Journal of Physics*, 1214.

Theiss, W., & Teiss, W. (2001). Scout Thin film Analysis Software Handbook, Hard and Software. *Aachen, Germany*, 54-57.

Thelen, A. (1981). Energy Related Optical coatings. *Optical coating laboratory*, 65-80.

Wang, Z., Chen, C., Wu, K., Chong, H., & Hui, Y. (2019). Transparent conductive oxides and their applications in near infrared Plasmonics.

Wanga, J., & Shi, D. (2017). Spectral selective and photothermal nano structured thin films for energy efficient windows. *Applied Energy 208*, 83-96.

Weis, & Martin. (2015). Transparent Electrodes for Flexible Organic Light-Emitting Diodes and Displays. . *Display and Imaging.*, 46-68.

Wooten, F. (1972). *Optical Properties of Solids.* New York: Academic Press.

Zhang, S. (2017). Study of fluorine-doped tin oxide (FTO) thin fims for photovoltaics applications. *Materials Universite Grenoble Alpes*.